Analysis and control of friction-induced oscillations in a continuous system

ARTICLE *in* JOURNAL OF VIBRATION AND CONTROL · FEBRUARY 2011

Impact Factor: 4.36 · DOI: 10.1177/1077546311403792

4 AUTHORS, INCLUDING:

Ashesh Saha
Indian Institute of Technology Kanpur
7 PUBLICATIONS **25** CITATIONS
SEE PROFILE

Bishakh Bhattacharya
Indian Institute of Technology Kanpur
62 PUBLICATIONS **150** CITATIONS
SEE PROFILE

Pankaj Wahi
Indian Institute of Technology Kanpur
54 PUBLICATIONS **284** CITATIONS
SEE PROFILE

Article

Journal of Vibration and Control
18(3) 467–480

DOI: 10.1177/1077546311403792
jvc.sagepub.com

Analysis and control of friction-induced oscillations in a continuous system

Ashesh Saha, Shashank Shekhar Pandey, Bishakh Bhattacharya and Pankaj Wahi

Abstract

We analyse and control friction-induced oscillations in a continuous system due to the drooping characteristics of the friction force. The model consists of a cantilever beam with an end mass that is in frictional contact with a rigid rotating disc. Time-delayed displacement feedback applied normal to the disc surface is used to control the vibrations. Linear stability analysis yields the stability boundary corresponding to the Hopf bifurcation point. Nonlinear analysis is performed to obtain conditions on the control parameters for which the nature of the bifurcation is subcritical such that these values can be avoided. The control parameters for effective quenching of the vibrations are obtained. An interesting regime of control parameters for which the system is stable for low and high velocities but unstable for intermediate velocities is also observed.

Keywords

Friction-induced oscillations, continuous system, Hopf bifurcation, time-delayed control force

Received: 24 November 2010; accepted: 11 January 2011

1. Introduction

Friction-induced oscillations have been a nemesis for many mechanical systems as they put restrictions on their operation. One can observe their presence in brake noise, railway wheel squeal, clutch chatter, machine tool chatter, vibrations in linkages with position control, etc. In this paper, we focus on a simple model consisting of a cantilever beam with an end mass in frictional contact with a rigid rotating disc. We also study the feasibility of controlling the vibration of the end mass using a delayed feedback.

Several mechanisms have been discussed in the literature for friction-induced vibrations. The most studied mechanism is the presence of an effective negative damping in the governing equations of motion (Hinrichs et al., 1998; Thomsen, 1999; Popp and Rudolph, 2004; Hetzler et al., 2007). This negative damping appears due to the drooping characteristic of the friction force in the low relative velocity regime. Various models have been proposed to account for a decrease in the friction force with increasing relative velocity and a brief discussion of these models can be found in (Saha et al., 2010). Mode coupling instability or binary flutter (an instability due to non-conservative displacement dependent forces) is another widely studied instability mechanism. Two structural modes of the system approach each other with the variation of a system parameter until their merger which subsequently results in an unstable mode. This mechanism does not require a variable frictional force to induce vibrations. Some minimal models for this instability have been discussed by Hoffman et al. (2002) and Hoffmann and Gaul (2003). Kinematic sprag–slip (Ibrahim, 1994; Hoffmann and Gaul, 2010), wherein the motions in the normal and tangential directions are coupled causing the normal force to vary with varying displacements, is yet another mechanism which can give rise to instability with a constant friction coefficient.

Different models have been studied for systems with friction-induced vibrations depending on the mechanism under consideration. The model most commonly used to understand the physics of the frictional instability consists of a mass on a moving belt. Friction-induced oscillations due to the drooping characteristic

Mechanical Engineering Department, Indian Institute of Technology, Kanpur, India

Corresponding author:
Ashesh Saha, Mechanical Engineering Department, Indian Institute of Technology, Kanpur 208016, India
Email: ashesh@iitk.ac.in

of the friction force are analysed by considering a single degree-of-freedom (DOF) spring–mass damper system on a moving belt (Hinrichs et al., 1998; Thomsen, 1999; Popp and Rudolph, 2004; Chatterjee, 2007; Hetzler et al., 2007; Saha et al., 2010; Saha and Wahi, 2010). However, a cantilever beam in frictional contact with a moving belt or a rigid rotating disc was considered by Popp and Stelter (1990) and Stelter (1992) to analyse the effect of drooping friction on the continuous system and they found periodic as well as chaotic motions. The mode-coupling instability is in general modelled by a two-DOF system on a moving belt (Hoffman et al., 2002; Hoffmann and Gaul, 2003). More complicated models for the mode-coupling instability have been considered in relation to brake squeal which includes the flexibility of the disc (Ouyang et al., 1998; Flint and Hulten, 2002; Shin et al., 2002). Ouyang et al. (1998) in their study found that the effective negative damping due to the drooping characteristics reduced the unstable region due to the mode-coupling instability. On the other hand, the kinematic sprag–slip instability is commonly modelled by an inclined cantilever beam in contact with a moving belt (Ibrahim, 1994; Hoffmann and Gaul, 2010). In this paper, we consider a model consisting of a cantilever beam with an end mass in contact with a rigid rotating disc to analyse the friction-induced instability due to the drooping characteristics. A more comprehensive model including the mode-coupling effect has not been attempted here for simplicity of analysis and ease of understanding the effects of the various parameters on the vibrations and its control.

The work reported in this paper is motivated by an experimental study by Nakae et al. (2010) on a mountain bike disc brake system which shows that squealing is primarily due to the drooping friction characteristics and the ensuing vibrations are in the plane of the disc surface. They have also identified vibrations involving out-of-plane disc motions referred to as chatter which occurs less frequently than squealing. However, the review paper by Kinkaid et al. (2003) on brake squeal suggests various (and often contradictory) major contributors to the squealing noise based on experimental findings. Some of these are squealing due to the in-plane vibrations of the disc (Matsuzaki and Izumihara, 1993; Dunlap et al., 1999), the vibrations of the pads and the brake calipers (Felske et al., 1978) and coupling of the various modes of the brake assembly (Murakami et al., 1984; Nishiwaki et al., 1989). Also, some recent experiments using a laboratory set-up to mimic automotive disc brakes support the mode-coupling phenomena as the main cause of brake squeal (Giannini et al., 2006; Giannini and Massi, 2008). It may be noted that the model considered in this study does not completely represent a brake squeal model since the rotating disc is considered to be rigid. Incorporation of the flexibility of the disc will incorporate possibilities of mode-coupling phenomenon and will correspond better with brake squeal. This extension will be attempted in future. Some other practical applications related to the current study involve frictional instability of the atomic force microscopy (AFM) tip during contact mode scanning, wiper blade noise, and the instability of the hard drive read–write mechanism (Sheng, 2008).

Researchers have adopted different strategies to control friction-induced vibrations. Thomsen (1999) used high-frequency tangential excitation in controlling friction-induced vibrations. Popp and Rudolph (2004) discussed the use of a dynamic vibration absorber as a passive means to control friction-induced stick–slip motion. Neubauer and Oleskiewicz (2008) used piezoceramics to control brake squeal with a PD feedback control while von Wagner et al. (2004) considered 'smart pads' and optimal control feedback. Time-delayed feedback control for frictional instability has been studied extensively (Chatterjee, 2007; Das and Mallik, 2006; Saha et al., 2010; Saha and Wahi, 2010). Neubauer et al. (2005) experimentally investigated the use of time-delayed velocity feedback to control friction-induced vibrations. To check the feasibility of controlling friction-induced vibrations in the simplified model considered in this study, we have used a time-delayed control force (as used by Chatterjee (2007) and Saha and Wahi (2010)) applied in the normal direction (as used by Neubauer et al. (2005) and Saha and Wahi (2010)).

The rest of the paper is organised as follows. In Section 2 we derive the mathematical model. The dynamics of the uncontrolled system is analysed in Section 3. Section 4 is devoted to the analysis of the controlled system and its behaviour. Some salient results for the controlled system are discussed in Section 5. Finally, we draw some conclusions in Section 6.

2. The mathematical model

To obtain an understanding of the basic mechanism of friction-induced vibrations in a continuous system, we consider a simplified system consisting of a flexible beam with an end mass that is in frictional contact with a rotating disc as shown in Figure 1. This simplified model is inspired by an experimental set-up developed in our laboratory to study friction-induced vibrations (Pandey, 2010). Our main objective is to study the oscillations of the end mass only. For that purpose, we only consider the bending modes of the flexible beam. We further simplify the problem by considering that the disc rotates in a single plane, i.e. we neglect the bending vibrations and the wobbling motion of the disc. This allows us to assume that the normal force at the interface between the mass and the

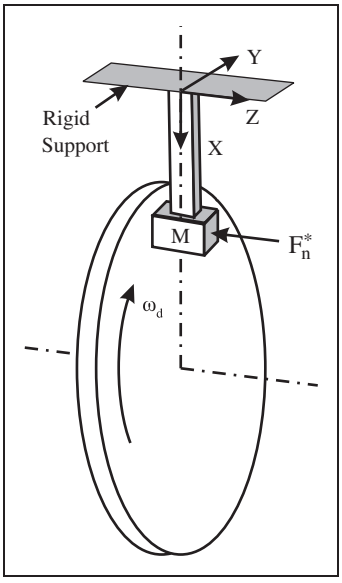

Figure 1. A flexible beam with an end mass on a rotating disc as a disc brake model.

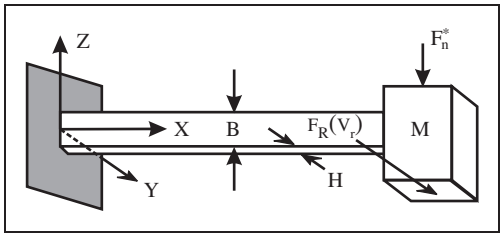

Figure 2. The flexible beam with end mass.

disc does not change during oscillations of the mass. We further neglect the in-plane torsional vibrations of the disc effectively making it a rigid body. Under these assumptions, the governing equation for the system corresponding to vibrations in the X–Y plane shown in Figure 2 is

$$E\,I\,\frac{\partial^4 V(X,t)}{\partial X^4}+\rho\,A\,\frac{\partial^2 V(X,t)}{\partial t^2}=0, \tag{1}$$

where E is the modulus of elasticity and ρ is the mass density of the beam material, $I=B\,H^3/12$ is the area moment of inertia of the beam cross section and $A=B\,H$ is the cross-sectional area. The boundary conditions for the beam equation (1) are $V(0,\,t)=0$, $\partial V/\partial X|_{X=0}=0$, $\partial^2 V/\partial X^2|_{X=L}=0$ and a non-homogenous boundary condition

$$M\left.\frac{\partial^2 V}{\partial t^2}\right|_{X=L}-E\,I\left.\frac{\partial^3 V}{\partial X^3}\right|_{X=L}=F_R(V_r), \tag{2}$$

where M is the mass of the slider, L is the length of the beam, $F_R(V_r)=F_n^*\,\mu(V_r)$ is the friction force, F_n^* is the total normal load acting on the end mass, $\mu\,(V_r)$ is the friction function, and V_r is the relative velocity between the disc and the end mass. In Figure 1, $F_n^*=N_0^*+F_{c1}^*$, where N_0^* is the externally applied normal load (the braking force) and F_{c1}^* is the control force. We consider a time-delayed control force of the following form (Chatterjee 2007; Saha and Wahi 2010)

$$F_{c1}^*=-K_{p1}^*\big[V(L,\,t)-V\big(L,\,t-T_1^*\big)\big], \tag{3}$$

where K_{p1}^* is the control gain, T_1^* is the time delay, and $V(L,\,t)$ is the deflection of the end mass. Using the non-dimensional quantities

$$x=\frac{X}{L},\quad y=\frac{V}{L},\quad \tau=\Omega\,t,\quad T_1=\Omega\,T_1^*,$$
$$\Omega=\sqrt{\frac{E\,I}{\rho\,A\,L^4}},\quad r_m=\frac{\rho\,A\,L}{M},$$
$$N_0=\frac{N_0^*}{M\,\Omega^2\,L},\quad K_{p1}=\frac{K_{p1}^*}{M\,\Omega^2},\quad v_d=\frac{V_d}{\Omega\,L},$$
$$v_r=v_d-\left.\frac{\partial y}{\partial\tau}\right|_{x=1},$$

the governing equation becomes

$$\frac{\partial^4 y}{\partial x^4}+\frac{\partial^2 y}{\partial\tau^2}=0 \tag{4}$$

with the boundary conditions: $y(0,\,\tau)=0$, $\partial y/\partial x|_{x=0}=0$, $\partial^2 y/\partial x^2|_{x=1}=0$ and

$$\left.\frac{\partial^2 y}{\partial\tau^2}\right|_{x=1}-r_m\left.\frac{\partial^3 y}{\partial x^3}\right|_{x=1}=\big(N_0+K_{p1}\,(y(1,\,\tau-T_1)-y(1,\,\tau))\big)\,\mu(v_r). \tag{5}$$

We consider the polynomial friction model (as used by Thomsen (1999)) for the analysis given by

$$\mu(v_r)=\mu_s\,\mathrm{sgn}(v_r)-\frac{3}{2}(\mu_s-\mu_m)\left(\frac{v_r}{v_m}-\frac{1}{3}\left(\frac{v_r}{v_m}\right)^3\right), \tag{6}$$

where v_r is the (non-dimensional) relative velocity between the mass and the disc, μ_s is the coefficient of static friction, and v_m is the velocity corresponding to μ_m, the minimum coefficient of kinetic friction ($\mu_m\le\mu_s$). The choice of the polynomial friction model is based on pure slipping motions observed in our experimental set-up (Pandey 2010). For ease of numerical integration $\mathrm{sgn}(v_r)$ is replaced by its smooth approximation $\tanh\,(\kappa\,v_r)$ with $\kappa=500$.

We further reduce the partial differential equation (4) to a set of ordinary differential equations (ODEs) using modal projections along similar lines as Stelter (1992) and Kelly (2000). We use the mode shapes of a cantilever beam with an end mass for the reduction

following the procedure outlined by Kelly (2000). The modal solution of Equation (4) can be written in the variable separable form as

$$y(x,\tau)=\sum_{i=1}^{\infty}\Psi_i(x)\,y_i(\tau). \tag{7}$$

Considering only a finite number of mode shapes we have $y(x,\tau)=\sum_{i=1}^{n}\Psi_i(x)\,y_i(\tau)$, where n is the number of mode shapes considered for the analysis. The mode shapes $\Psi_i(x)$ are

$$\begin{aligned}\Psi_i(x)=C_i\,&((\cos(p_i)+\cosh(p_i))\\&(\sin(p_i\,x)-\sinh(p_i\,x))\;-(\sin(p_i)+\sinh(p_i))\\&(\cos(p_i\,x)-\cosh(p_i\,x))),\quad i=1,2,\ldots,n,\end{aligned} \tag{8}$$

where

$$C_i=\frac{p_i}{\sqrt{r_m\,(1+\cos(p_i)\,\cosh(p_i))^2+p_i^2\,(\sin(p_i)+\sinh(p_i))^2}}. \tag{9}$$

The natural frequencies p_i in Equation (8) are obtained from the frequency equation

$$\begin{aligned}1+\cos(p_i)\,\cosh(p_i)+\frac{p_i}{r_m}\,&(\cos(p_i)\,\sinh(p_i)\\&-\sin(p_i)\,\cosh(p_i))=0.\end{aligned} \tag{10}$$

The natural frequencies in the dimensional form are $\omega_i=p_i^2\,\Omega$. The mode shapes $\Psi_i(x)$ in Equation (8) satisfy the orthonormality properties

$$\frac{1}{r_m}\left(\Psi_i(1)\,\Psi_j(1)\right)+\int_0^1\Psi_i(x)\,\Psi_j(x)\,dx=\delta_{ij}, \tag{11a}$$

$$\frac{p_i^4}{r_m}\left(\Psi_i(1)\,\Psi_j(1)\right)+\int_0^1\Psi_j(x)\,\frac{d^4\Psi_i(x)}{dx^4}\,dx=p_i^4\,\delta_{ij}. \tag{11b}$$

These mode shapes obviously satisfy the governing equation along with the homogeneous boundary conditions, i.e., $d^4\Psi_i/dx^4-p_i^4\,\Psi_i=0$, $\Psi_i(0)=0$, $d\Psi_i/dx|_{x=0}=0$, $d^2\Psi_i/dx^2|_{x=1}=0$. The relationship obtained for the corresponding nonhomogeneous boundary condition is

$$\left.\frac{d^3\Psi_i}{dx^3}\right|_{x=1}=-\frac{p_i^4}{r_m}\,\Psi_i(1). \tag{12}$$

Substituting the modal solution given by Equation (7) into Equation (4) results in

$$\sum_{i=1}^{n}\frac{d^4\Psi_i}{dx^4}\,y_i+\sum_{i=1}^{n}\Psi_i\,\frac{d^2y_i}{d\tau^2}=0. \tag{13}$$

Multiplying Equation (13) by Ψ_j and integrating over the domain [0, 1], we obtain

$$\begin{aligned}\sum_{i=1}^{n}y_i\int_0^1\Psi_j(x)\,\frac{d^4\Psi_i(x)}{dx^4}\,dx\\+\sum_{i=1}^{n}\frac{d^2y_i}{d\tau^2}\int_0^1\Psi_i(x)\,\Psi_j(x)\,dx=0\end{aligned} \tag{14}$$

that reduces to (using the orthonormality conditions given by Equations (11a) and (11b))

$$\begin{aligned}\sum_{i=1}^{n}p_i^4\,y_i\left(\delta_{ij}-\frac{1}{r_m}\left(\Psi_i(1)\,\Psi_j(1)\right)\right)\\+\sum_{i=1}^{n}\frac{d^2y_i}{d\tau^2}\left(\delta_{ij}-\frac{1}{r_m}\left(\Psi_i(1)\,\Psi_j(1)\right)\right)=0,\end{aligned} \tag{15}$$

$$\Rightarrow\frac{d^2y_j}{d\tau^2}+p_j^4\,y_j=\frac{1}{r_m}\sum_{i=1}^{n}\left(\frac{d^2y_i}{d\tau^2}+p_i^4\,y_i\right)\Psi_{i1}\,\Psi_{j1},\quad j=1,\ldots,n, \tag{16}$$

where $\Psi_{i1}=\Psi_i(1)$ and $\Psi_{j1}=\Psi_j(1)$. The terms on the right-hand side of Equation (16) can be evaluated using the non-homogenous boundary condition. To this end, we substitute the modal solution, i.e. Equation (7) into Equation (5) and obtain

$$\begin{aligned}\sum_{i=1}^{n}\Psi_{i1}\,\frac{d^2y_i}{d\tau^2}-r_m\sum_{i=1}^{n}\left.\frac{d^3\Psi_i}{dx^3}\right|_{x=1}y_i\\=\left(N_0+K_{p1}\left(\sum_{i=1}^{n}\Psi_{i1}\,(y_i)_{T_1}-\sum_{i=1}^{n}\Psi_{i1}\,y_i\right)\right)\mu(v_r),\end{aligned} \tag{17}$$

where $(y_i)_{T_1}=y_i(\tau-T_1)$ and $v_r=v_d-\sum_{i=1}^{n}\Psi_{i1}\,y_i'$. Equation (17) can be simplified using Equation (12) to

$$\begin{aligned}\sum_{i=1}^{n}\left(\frac{d^2y_i}{d\tau^2}+p_i^4\,y_i\right)\Psi_{i1}\\=\left(N_0+K_{p1}\left(\sum_{i=1}^{n}\Psi_{i1}\,(y_i)_{T_1}-\sum_{i=1}^{n}\Psi_{i1}\,y_i\right)\right)\mu(v_r)\end{aligned} \tag{18}$$

which gives us the right-hand side of Equation (16). Substitution of Equation (18) into Equation (16) yields

$$\begin{aligned}\frac{d^2y_j}{d\tau^2}+p_j^4\,y_j\\=\frac{\Psi_{j1}}{r_m}\left(N_0+K_{p1}\left(\sum_{i=1}^{n}\Psi_{i1}\,(y_i)_{T_1}-\sum_{i=1}^{n}\Psi_{i1}\,y_i\right)\right)\mu(v_r),\\j=1,\ldots,n.\end{aligned} \tag{19}$$

Considering only the first mode ($n=1$), Equation (19) reduces to

$$\frac{d^2y_1}{d\tau^2}+p_1^4\,y_1=\frac{\Psi_{11}}{r_m}\left(N_0+K_{p1}\,\Psi_{11}\left((y_1)_{T_1}-y_1\right)\right)\mu(v_r), \tag{20}$$

where $v_r=v_d-\Psi_{11}\,(dy_1/d\tau)$. If we consider the first two modes ($n=2$) for the analysis, we obtain the following coupled equations

$$\frac{d^2y_1}{d\tau^2}+p_1^4\,y_1=\frac{\Psi_{11}}{r_m}\left(N_0+K_{p1}\left(\Psi_{11}\left((y_1)_{T_1}-y_1\right)+\Psi_{21}\left((y_2)_{T_1}-y_2\right)\right)\right)\mu(v_r), \tag{21a}$$

$$\frac{d^2y_2}{d\tau^2}+p_2^4\,y_2=\frac{\Psi_{21}}{r_m}\left(N_0+K_{p1}\left(\Psi_{11}\left((y_1)_{T_1}-y_1\right)+\Psi_{21}\left((y_2)_{T_1}-y_2\right)\right)\right)\mu(v_r), \tag{21b}$$

where $v_r=v_d-(\Psi_{11}(dy_1/d\tau)+\Psi_{21}(dy_2/d\tau))$. We represent the displacement and velocity of the mass as $y_m=\sum_{i=1}^{n}\Psi_{i1}\,y_i$ and $y'_m=\sum_{i=1}^{n}\Psi_{i1}\,y'_i$, where 'prime' denotes the derivative with respective to the non-dimensional time τ.

The continuous system can have a countably infinite number of mode shapes. However, the dynamics for practical situations is mostly governed by finitely many mode shapes. Hence, it is desirable to obtain the minimum number of mode shapes to accurately capture the dynamics of interest. For this purpose, the phase plot of the limit cycle for the uncontrolled system ($K_{p1}=0$) for a standard set of parameter values $v_d=0.1$, $r_m=0.8$, $N_0=0.02$, $\mu_s=0.4$, $\mu_m=0.25$ and $v_m=0.2$ is presented considering only the first mode and the first two modes in Figure 3. It can be observed from Figure 3 that the limit cycle obtained by considering the first two modes does not deviate much from that obtained by considering only the first mode. Therefore, we will only consider the first mode approximation for our future analysis.

The equilibrium or steady-state of Equation (20) is

$$y_{1s}=\frac{q_1\,N_0\,\mu(v_{\rm d})}{\omega_{n1}^2}, \tag{22}$$

where $q_1=\Psi_{11}/r_m$ and $\omega_{n1}^2=p_1^4$. Shifting the origin to the equilibrium state by introducing $z_1=y_1-y_{1s}$ ($z'_1=y'_1$, $z''_1=y''_1$), we obtain the non-dimensional equation in the shifted coordinate z_1 as

$$z''_1+\omega_{n1}^2\,z_1=q_1\,N_0\,(\mu(v_r)-\mu(v_{\rm d}))+q_1\,\Psi_{11}\,K_{p1}\left((z_1)_{T_1}-z_1\right)\mu(v_r), \tag{23}$$

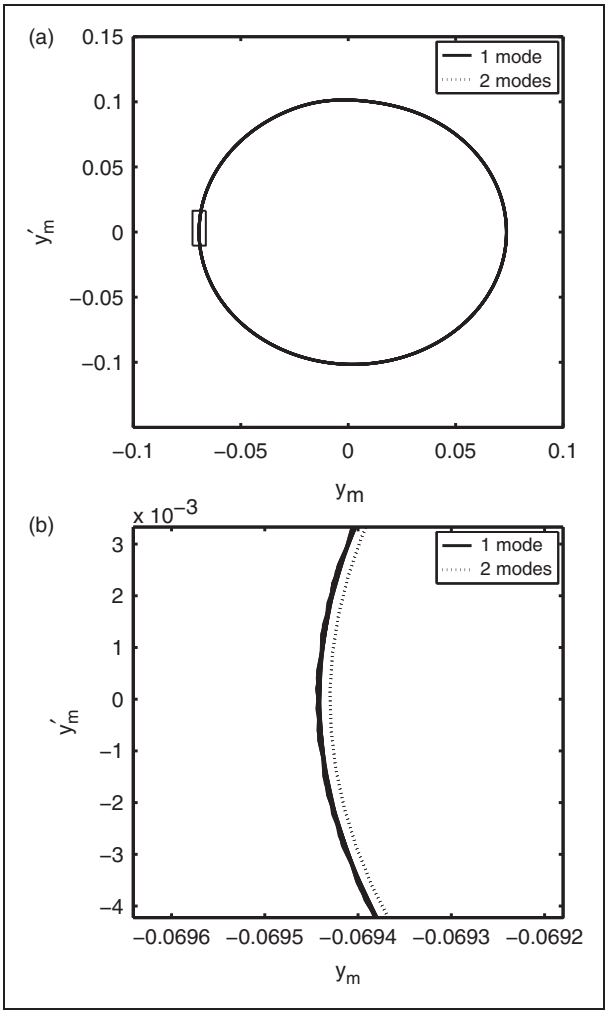

Figure 3. (a) Phase-plane plot. (b) A magnified view of (a) to clearly show results from first two mode shapes. Parameters: $v_d=0.1$, $r_m=0.8$, $N_0=0.02$, $\mu_s=0.4$, $\mu_m=0.25$, $v_m=0.2$, and $\kappa=500$.

where $(z_1)_{T_1}=z_1(\tau-T_1)$ and $v_r=v_d-\Psi_{11}\,z'_1$. For the analytical study, we consider only pure slipping motions ($\mathrm{sgn}(v_r)=1$) for which Equation (23) can be modified to

$$z''_1+\omega_{n1}^2\,z_1=\;q_1\left(N_0+\Psi_{11}\,K_{p1}\left((z_1)_{T_1}-z_1\right)\right)\left(B_1\,z'_1+B_2\,z_1'^2+B_3\,z_1'^3\right)+q_1\,\Psi_{11}\,K_{p1}\left((z_1)_{T_1}-z_1\right)\mu(v_{\rm d}), \tag{24}$$

where $B_1=\Psi_{11}\,\alpha_1\left(1-v_d^2/v_m^2\right)$, $B_2=\Psi_{11}^2\,\alpha_1\,v_d/v_m^2$, $B_3=\frac{1}{3}(\Psi_{11}^3\,\alpha_1/3\,v_m^2)$, $\mu(v_{\rm d})=\mu_s+\alpha_1\,v_d^3/3\,v_m^2-\alpha_1\,v_d$, $\alpha_1=\frac{3}{2}\,((\mu_s-\mu_m)/v_m)$.

3. Dynamics of the uncontrolled system

In this section, we study the dynamics of the uncontrolled system ($K_{p1}=0$) in some detail. For this case, Equation (23) reduces to

$$z_1'' + \omega_{n1}^2 z_1 = q_1 N_0 (\mu(v_r) - \mu(v_d)). \tag{25}$$

As mentioned earlier, we consider only pure slipping motion for the analytical study and the relevant equation (from Equation (24)) is

$$z_1'' + \omega_{n1}^2 z_1 = q_1 N_0 \left(B_1 z_1' + B_2 z_1'^2 + B_3 z_1'^3\right). \tag{26}$$

The linearized form of Equation (26) is

$$z_1'' - q_1 N_0 B_1 z_1' + \omega_{n1}^2 z_1 = 0. \tag{27}$$

Equation (27) has the same form as a damped harmonic oscillator and the stability boundary (Hopf point) separating the stable and unstable equilibrium is given by $B_1=0$ (equivalent to zero damping) which corresponds to $v_d=v_m$. When $v_d<v_m$, $B_1>0$ and the equilibrium is unstable. On the other hand, for $v_d>v_m$ we have $B_1<0$ and thus the equilibrium is stable. We next perform a nonlinear analysis to obtain an estimate of the amplitudes of the resulting vibrations in the linearly unstable regime and to affirm the nature of the bifurcation which should be supercritical (Thomsen 1999; Saha et al. 2010).

3.1. Nonlinear analysis using the method of averaging

To perform averaging we first convert Equation (26) into the standard form as follows

$$z_1'' + \omega_{n1}^2 z_1 = \epsilon f\left(z_1(\tau), z_1'(\tau)\right), \quad 0 < \epsilon \ll 1, \tag{28}$$

where

$$\epsilon f\left(z_1(\tau), z_1'(\tau)\right) = q_1 N_0 \left(B_1 z_1' + B_2 z_1'^2 + B_3 z_1'^3\right). \tag{29}$$

For $\epsilon=0$, the system is a simple harmonic oscillator (SHO). Accordingly, for $\epsilon\neq 0$ the solution is assumed to be

$$z_1 = A_{1un}(\tau)\cos(\omega_{n1}\tau + \varphi_1(\tau)), \tag{30a}$$

$$z_1' = -\omega_{n1} A_{1un}(\tau)\sin(\omega_{n1}\tau + \varphi_1(\tau)), \tag{30b}$$

where the amplitude A_{1un} and the phase φ_1 are slowly varying functions of time τ. Following the standard procedure for the method of averaging (Sanders et al. 2007), we get the following amplitude equation:

$$A_{1un}' = (L_{1a})_{un} A_{1un} + (NL_{1a})_{un} A_{1un}^3, \tag{31}$$

where

$$(L_{1a})_{un} = \frac{q_1 N_0}{2} B_1, \tag{32a}$$

$$(NL_{1a})_{un} = \frac{3 q_1 N_0 \omega_{n1}^2}{8} B_3. \tag{32b}$$

Equating A_{1un}' to zero we obtain the fixed points as: (i) $A_{1un}=0$ which is the steady state or equilibrium of the system and (ii) $A_{1un} = \sqrt{-(L_{1a})_{un}/(NL_{1a})_{un}}$ which is the amplitude of the limit cycle. $(L_{1a})_{un}=0 \Rightarrow B_1=0$ gives us the Hopf point where the stability of the equilibrium changes. This gives us the Hopf point as $v_{dao}=v_m$, which is exactly the same as obtained from the linear stability analysis discussed above. The nature of the Hopf bifurcation is determined from the sign of $(NL_{1a})_{un}$ or equivalently the sign of B_3 which is negative. Thus, the nature of Hopf bifurcation is supercritical. Therefore, considering v_d as the bifurcation parameter, the equilibrium $A_{1un}=0$ is globally stable for $v_d>v_{dao}$. Substituting for B_1 and B_3 in Equation (32) and the resulting expressions in the solution for the limit cycle amplitude A_{1un}, we obtain

$$A_{1un} = \frac{2}{\Psi_{11}\omega_{n1}}\sqrt{v_m^2 - v_d^2}. \tag{33}$$

It may be noted that in all of the above expressions the subscripts 'a', 'un' and 'o' denote the method of averaging, the uncontrolled system and the Hopf point, respectively. We can infer from Equation (33) that the amplitude of the limit cycle for a given v_d depends on the parameters Ψ_{11} and ω_{n1} which themselves depend on the mass ratio r_m, and the velocity corresponding to the minimum kinetic coefficient v_m while it is independent of the normal load N_0 and the friction coefficients μ_s and μ_m. These analytical findings are verified against numerical simulations in the next subsection by considering several bifurcation diagrams with v_d as the bifurcation parameter. We also obtain the range of parameters for which the assumption of small beam deflections used in obtaining the Euler–Bernoulli beam equation (1) is valid.

3.2. Parametric studies of the uncontrolled system

We analyse the effect of different system parameters on the behaviour of the system through numerically

generated bifurcation diagrams. These bifurcation diagrams have been obtained using a fixed arc-length based continuation scheme discussed by Wahi and Chatterjee (2008). In the bifurcation diagrams, the maximum displacement ($(y_m)_{\max}$) of the end mass is plotted as a function of the disc velocity at the point of contact with the end mass (v_d).

We first consider the effect of the normal load N_0 which is equivalent to the braking force in Figure 4. It can be observed from Figure 4 that the amplitude of the vibration for any given v_d increases with an increase in N_0 in contrast to the analytical finding of the previous section. However, the variation in the amplitude is not significant for major portions of the pure-slipping regime and this variation can be obtained analytically using a higher-order analytical calculation which is not attempted here. An interesting fact to note from Figure 4 is that the disc velocity v_d corresponding to the impending stick–slip motion does not vary with a variation in N_0 and hence the regions with pure slipping and stick–slip motions are unaffected by the normal load.

The bifurcation diagrams in Figure 5 are plotted for different v_m values. As mentioned earlier, v_m is the velocity corresponding to the minimum kinetic friction coefficient μ_m and depends on the frictional interface. It may be noted that the friction parameters cannot be varied in a continuous fashion in experiments to study their effect. Hence, these diagrams are generated basically to obtain the parameter sets for which our model based on small deflection theory is valid. Figure 5 shows that the amplitude of the stick–slip limit cycle for a given v_d is independent of v_m whenever such motions exist. However, the qualitative nature of the solutions for a given v_d depends on v_m, e.g. for a disc velocity of $v_d = 0.14$, the motion is stick–slip type for $v_m = 0.2$, pure slip for $v_m = 0.15$ and no vibrations exist for $v_m = 0.1$. As expected, the maximum amplitude (at impending stick–slip motion) becomes larger as the value of v_m is increased.

As noted in our previous discussion, the mass ratio r_m acts as a crucial parameter since it affects the eigenvalue $\omega_{n1} = p_1^2$ as well as the mode shapes (and, hence, Ψ_{11}). However, the effect of r_m on these parameters is non-trivial making equation (33) practically useless for the study of its effect on the amplitude of the vibrations. The effect of the variation in r_m on the resulting vibrations is depicted in Figure 6 that shows an increase in the maximum displacement with a decrease in r_m. It can be noted from this figure that the maximum displacement becomes quite high for smaller r_m values causing a breakdown of the validity of our model. However, the qualitative nature of the solutions are independent of r_m.

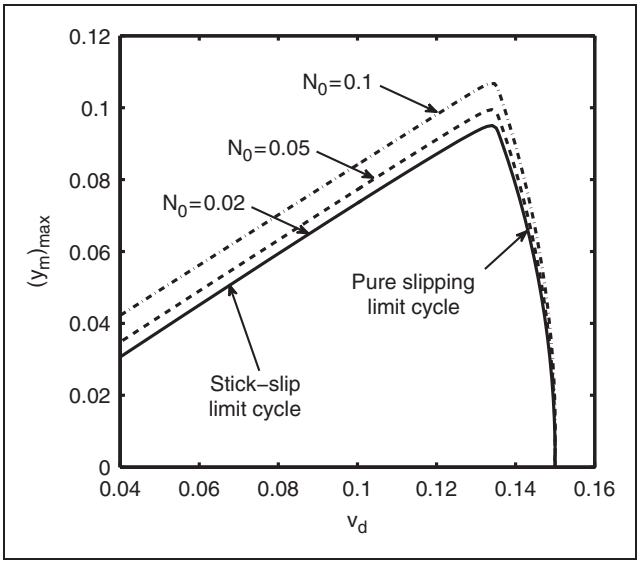

Figure 4. Effect of N_0 on the bifurcation diagram with v_d as the bifurcation parameter. Parameters: $\mu_s = 0.4$, $\mu_m = 0.25$, $v_m = 0.15$, $r_m = 0.8$ and $\kappa = 500$.

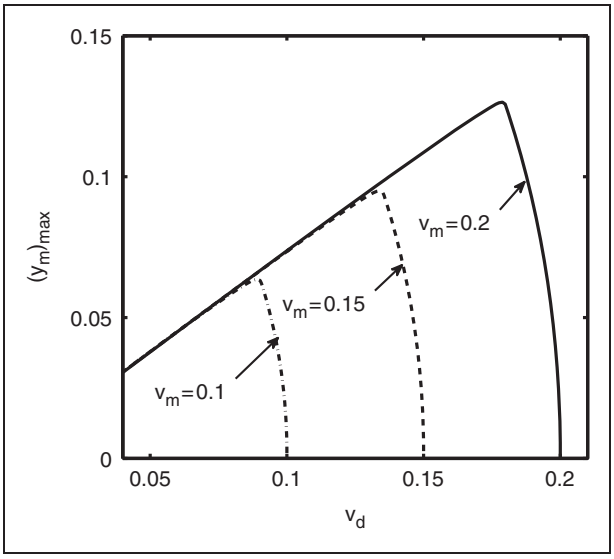

Figure 5. Effect of v_m on the bifurcation diagram with v_d as the bifurcation parameter. Parameters: $\mu_s = 0.4$, $\mu_m = 0.25$, $r_m = 0.8$, $N_0 = 0.02$ and $\kappa = 500$.

Before proceeding further, we ascertain the range of the parameter values for which the Euler–Bernoulli beam equations are valid. For this consideration, we assume that the beam deflections are small until they are less than 0.15 times the length of the beam. Accordingly, our model is valid until $(y_m)_{\max} = 0.15$. Based on this criterion and the parametric studies in this section, we choose the parameter set for our further analysis as $\mu_s = 0.4$, $\mu_m = 0.25$, $v_m = 0.2$, $N_0 = 0.02$ and

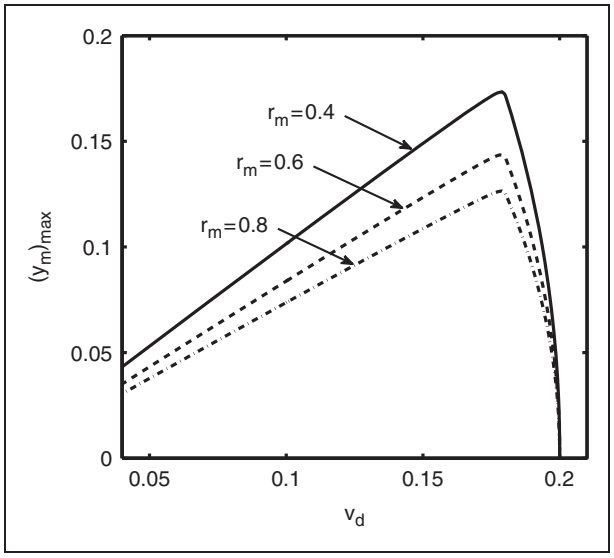

Figure 6. Effect of r_m on the bifurcation diagram with v_d as the bifurcation parameter. Parameters: $\mu_s = 0.4$, $\mu_m = 0.25$, $v_m = 0.2$, $N_0 = 0.02$ and $\kappa = 500$.

$r_m = 0.8$. For this parameter set, the maximum deflection of the end mass $(y_m)_{\max}$ is approximately 0.12 which falls well within the small deflection limit. For $r_m = 0.8$, we have $p_1 = 1.1918$, $\omega_{n1} = p_1^2 = 1.4204$ and $\Psi_{11} = 0.8199$.

4. The controlled system and its behaviour

In this section, we analyse the system given by Equation (23) which involves the control force as well. We start with a linear stability analysis to obtain the stability boundary corresponding to the Hopf bifurcation point.

4.1. Linear stability analysis

The linearized equation about the equilibrium point $z_1 = 0$ is

$$z_1'' + \omega_{n1}^2 z_1 = q_1 N_0 B_1 z_1' + q_1 \Psi_{11} K_{p1} (z_1(\tau - T_1) - z_1) \mu(v_d). \quad (34)$$

Substituting $z_1 = c_0 e^{s\tau}$, we obtain the corresponding characteristic equation as

$$s^2 + \omega_{n1}^2 = q_1 N_0 B_1 s + q_1 \mu(v_d) \Psi_{11} K_{p1} \left(e^{-s T_1} - 1\right). \quad (35)$$

On the stability boundary there is a purely imaginary root, i.e. $s = \pm j\,\omega$, where ω is the frequency of the ensuing periodic oscillation. Accordingly we substitute $s = \pm j\,\omega$ in Equation (35) and separate the real and imaginary parts to obtain

$$-\omega^2 + \omega_{n1}^2 = q_1 \mu(v_d) \Psi_{11} K_{p1} (\cos(\omega T_1) - 1), \quad (36a)$$

$$\omega q_1 B_1 N_0 = q_1 \mu(v_d) \Psi_{11} K_{p1} \sin(\omega T_1). \quad (36b)$$

Solving Equations (36a) and (36b) we get the critical values of the control parameters K_{p1} and T_1 in terms of ω for a given value of the disc velocity v_d as

$$K_{p1o} = -\frac{N_0^2 B_1^2 \omega^2 q_1^2 + \omega^4 - 2\omega^2 \omega_{n1}^2 + \omega_{n1}^4}{2 q_1 \mu(v_d) \Psi_{11} \left(\omega_{n1}^2 - \omega^2\right)}, \quad (37a)$$

$$T_{1o} = \frac{2}{\omega} \tan^{-1}\left[\frac{\omega^2 - \omega_{n1}^2}{\omega q_1 N_0 B_1}\right]. \quad (37b)$$

Considering the control gain K_{p1} as our bifurcation parameter, we determine the stable and unstable regions by checking the transversality condition, i.e.

$$R_1(\omega_c, K_{p1o}) = \mathrm{sgn}\left[Re\left(\frac{ds}{dK_{p1}}\Big|_{j\omega_c, K_{p1o}}\right)\right] = \mathrm{sgn}\big[q_1^2 \mu(v_d)(\cos(\omega_c T_{1o}) - 1) \left(\mu(v_d) \Psi_{11} K_{p1o} T_{1o} \cos(\omega_c T_{1o}) - q_1 N_0 B_1\right) + \left(q_1^2 \mu(v_d)^2 \Psi_{11} K_{p1o} T_{1o} \sin^2(\omega_c T_{1o})\right)\big]. \quad (38a)$$

The equilibrium is stable for $K_{p1} > K_{p1o}$ if $R_1 < 0$ and unstable for $K_{p1} > K_{p1o}$ if $R_1 > 0$. It was shown by Saha and Wahi (2010) that a linear control force in the normal direction can change the nature of the bifurcation. Hence, a nonlinear analysis is required to ascertain the range of the control parameters for which the bifurcation is supercritical in nature. This analysis is our next step.

4.2. Nonlinear analysis by the method of averaging

We use the method of averaging to obtain a qualitative understanding of the time-delayed control on the stability of the system owing to the simplicity of the obtained expressions (Saha et al. 2010). We first rewrite Equation (24) in the standard form as follows

$$z_1'' + \omega_{n1}^2 z_1 = \epsilon f\left(z_1(\tau), z_1'(\tau), (z_1)_{T_1}\right), \quad 0 < \epsilon \ll 1, \quad (39)$$

where $(z_1)_{T_1} = z_1(\tau - T_1)$ and

$$\epsilon f\left(z_1(\tau), z_1'(\tau), (z_1)_{T_1}\right) = q_1 \left[N_0 + \Psi_{11} K_{p1}\left((z_1)_{T_1} - z_1\right)\right] \left[B_1 z_1' + B_2 z_1'^2 + B_3 z_1'^3\right] + q_1 \Psi_{11} K_{p1}\left((z_1)_{T_1} - z_1\right)\mu(v_d). \quad (40)$$

Following the standard procedure for the averaging of systems with delays outlined in Saha et al. (2010), Saha and Wahi (2010) and Wahi and Chatterjee (2004), we obtain the following amplitude equation

$$A_1' = L_{1a}\, A_1 + NL_{1a}\, A_1^3, \tag{41}$$

where

$$L_{1a} = q_1\left[\frac{N_0\, B_1\, \omega_{n1} - \Psi_{11}\, K_{p1}\, \mu(v_{\mathrm{d}})\sin(\omega_{n1}\, T_1)}{2\,\omega_{n1}}\right], \tag{42a}$$

$$NL_{1a} = \frac{3\,q_1}{4}\left[\frac{N_0\, B_3\, \omega_{n1}^3 - \Psi_{11}\, K_{p1}\, B_2\, \omega_{n1}^2 \sin(\omega_{n1}\, T_1)}{2\,\omega_{n1}}\right]. \tag{42b}$$

To obtain the amplitudes of the limit cycles which are the non-trivial fixed points of Equation (41), we equate A_1' to zero and obtain $A_{1a} = \sqrt{-L_{1a}/NL_{1a}}$. Clearly the existence of a limit cycle demands the sign of L_{1a} and NL_{1a} to differ. The stability of the solutions are determined by the sign of the derivative

$$\frac{\mathrm{d}A_1'}{\mathrm{d}A_1} = L_{1a} + 3\, NL_{1a}\, A_1^2 \tag{43}$$

evaluated at the fixed points of Equation (41). The derivative given by Equation (43) at the fixed points are $\mathrm{d}A_1'/\mathrm{d}A_1\big|_{A_1=0} = L_{1a}$ and $\mathrm{d}A_1'/\mathrm{d}A_1\big|_{A_1=A_{1a}} = -2\,L_{1a}$, respectively. The sign of these two derivatives leads to the following two cases:

1. When $L_{1a} < 0$, $\mathrm{d}A_1'/\mathrm{d}A_1\big|_{A_1=0} < 0$ and $\mathrm{d}A_1'/\mathrm{d}A_1\big|_{A_1=A_{1a}} > 0$. This implies that the steady state is stable and the limit cycle, if it exists, is unstable. The limit cycle exists only if $NL_{1a} > 0$. The coexistence of an unstable limit cycle with a stable equilibrium signifies a subcritical Hopf bifurcation.
2. When $L_{1a} > 0$, $\mathrm{d}A_1'/\mathrm{d}A_1\big|_{A_1=0} > 0$ and $\mathrm{d}A_1'/\mathrm{d}A_1\big|_{A_1=A_{1a}} < 0$. In this case the equilibrium is unstable. The existence of a stable limit cycle demands $NL_{1a} < 0$ and the bifurcation is supercritical in nature.

Since the control parameters (K_{p1} and T_1) affect both the L_{1a} and NL_{1a} terms, the control force can change the nature of the bifurcation from supercritical to subcritical. This is undesirable because a stable large-amplitude stick–slip limit cycle coexists with a stable equilibrium close to the stability boundary for a subcritical bifurcation. This makes the system prone to vibrations even for $v_d > v_{dao}$. Therefore, we should obtain the criticality point where the nature of the bifurcation changes and avoid control parameters which induce subcritical Hopf bifurcations in the system. To this end, we first obtain the disc velocity v_d at the Hopf point corresponding to a given set of control parameters K_{p1} and T_1. Equating L_{1a} to zero yields

$$a_3\, v_d^3 + a_2\, v_d^2 + a_1\, v_d + a_0 = 0, \tag{44}$$

where $a_0 = \mu_s\, K_{p1}\, \sin(\omega_{n1}\, T_1) - N_0\, \omega_{n1}\, \alpha_1$, $a_1 = -\alpha_1\, K_{p1}\, \sin(\omega_{n1}\, T_1)$, $a_2 = N_0\, \omega_{n1}\, \alpha_1 / v_m^2$ and $a_3 = (\alpha_1/3\, v_m^2)\, K_{p1}\, \sin(\omega_{n1}\, T_1)$. The real positive roots of the cubic equation (44) give us the critical disc velocities v_{dao}. The condition $L_{1a} = 0$ can also be written as

$$K_{p1ao}\, \sin(\omega_{n1}\, T_{1ao}) = \frac{N_0\, \omega_{n1}\, \alpha_1 \left(1 - \left(\frac{v_{dao}}{v_m}\right)^2\right)}{\mu_s + \frac{\alpha_1}{3\, v_m^2}\, v_{dao}^3 - \alpha_1\, v_{dao}}. \tag{45}$$

The condition for a subcritical bifurcation ($NL_{1a} > 0$) is possible in Equation (42b) only when $\sin(\omega_{n1}\, T_1) < 0$ giving us an initial estimate of the undesirable delay range as $\pi\ /\omega_{n1} < T_1 < 2\ \pi\ /\omega_{n1}$. The condition $NL_{1a} > 0$ further results in the inequality

$$v_{dao} < -\frac{N_0\, \omega_{n1}}{3\, K_{p1ao}\, \sin(\omega_{n1}\, T_{1ao})}. \tag{46}$$

Substituting Equation (45) into Equation (46), we finally obtain the condition for subcriticality as

$$v_{dao} > \left(\frac{3}{2}\,\frac{\mu_s\, v_m^2}{\alpha_1}\right)^{1/3} = v_{dacr}, \tag{47}$$

where v_{dacr} is the disc velocity corresponding to the criticality point. Now, substituting $\alpha_1 = \frac{3}{2}\,((\mu_s - \mu_m)/v_m)$ into the expression for v_{dacr} we obtain

$$v_{dacr} = \left(\frac{\mu_s}{\mu_s - \mu_m}\right)^{1/3} v_m. \tag{48}$$

Clearly, $v_{dacr} > v_m$ which further implies that $v_{dao} > v_m$. Thus, subcritical bifurcations are obtained only when the critical disc velocity for the controlled case becomes higher than that for the uncontrolled case. The set of control parameters corresponding to this case is anyway undesirable since the control force is destabilising the otherwise stable system. Hence, for the choice of parameters for which the control is effective we will not obtain subcritical bifurcations.

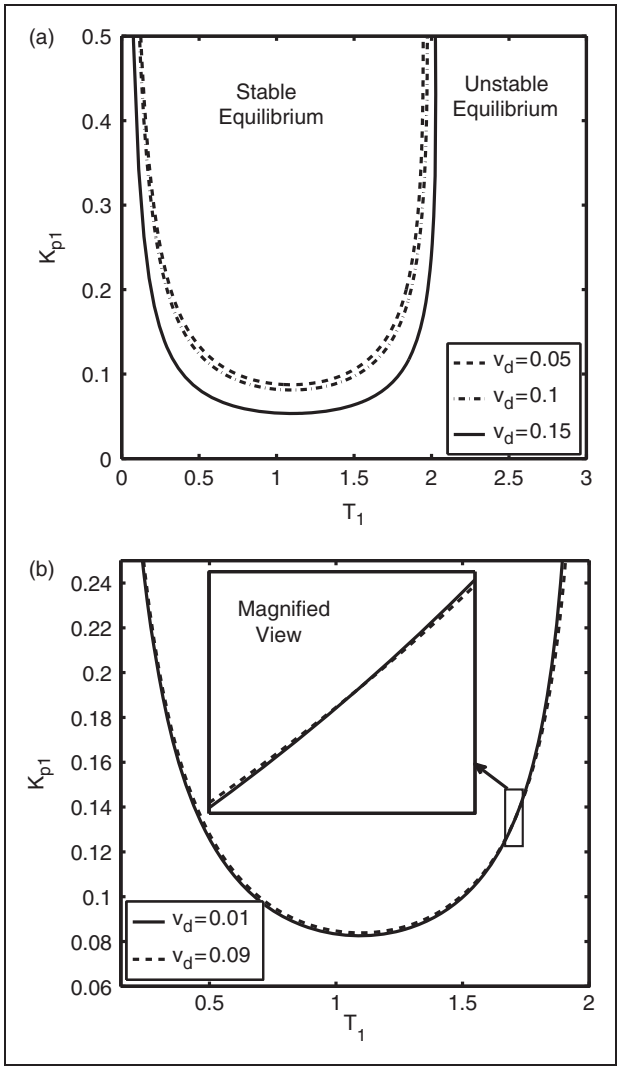

Figure 7. Stability boundaries in the plane of control parameters (K_{p1} and T_1) for different v_d. Crossing of the two stability boundaries corresponding to two different v_d is shown in the inset of (b). Parameters: $\mu_s = 0.4$, $\mu_m = 0.25$, $v_m = 0.2$, $r_m = 0.8$ and $N_0 = 0.02$.

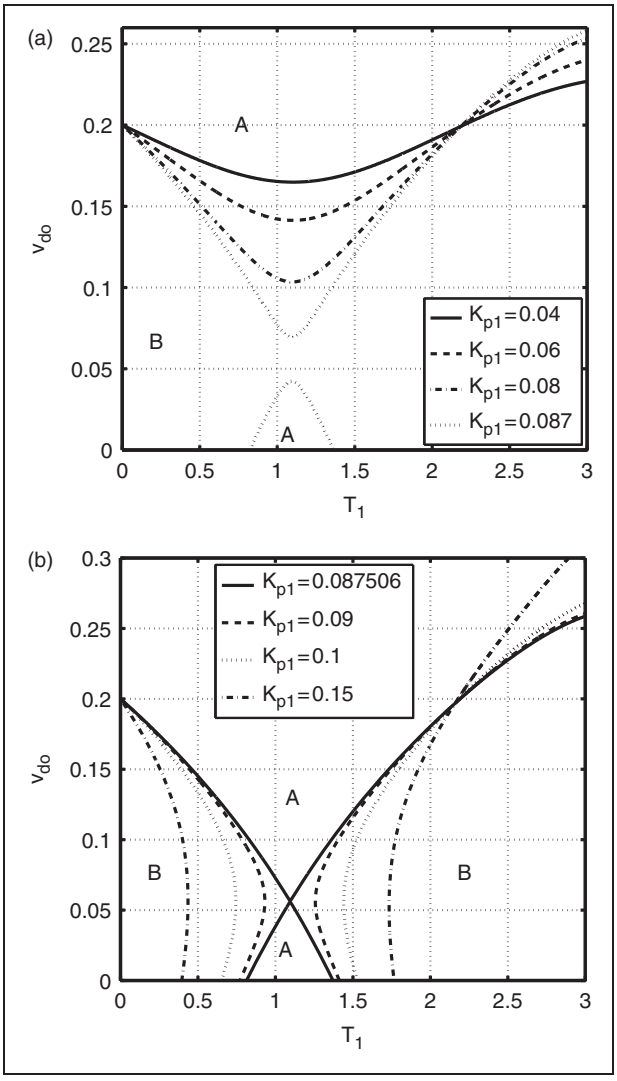

Figure 8. Time delay T_1 vs. critical disc velocity v_{do} for different control gain K_{p1}. (A) Stable equilibrium. (B) Unstable equilibrium. Parameters: $\mu_s = 0.4$, $\mu_m = 0.25$, $v_m = 0.2$, $r_m = 0.8$ and $N_0 = 0.02$.

5. Results and discussions for the controlled system

We first consider the linear stability boundaries in the control parameter plane (T_1 vs. K_{p1} plane) given by Equations (37) in Figure 7. The stability boundaries are shown in Figure 7 for different disc velocities v_d which correspond to various locations of the end mass on the disc or different RPM of the motor for our experimental set-up. The disc velocities are chosen to be less than the uncontrolled system critical disc velocity such that the control is effective. It is observed from Figure 7(a) that for higher disc velocities the stable region increases as expected. However, Figure 7(b) shows intersection of two stability boundaries for two different disc velocities as is evident from the inset. Therefore, there could be two distinct critical disc velocities for a particular set of control parameters corresponding to the intersection point. To fully understand the implication of this intersection, we analyse the critical disc velocity v_{do} as a function of the control parameter T_1.

Figure 8 depicts the variation in v_{do} with T_1 for different values of K_{p1} obtained by numerically solving equations (36). It is observed that the critical disc velocity v_{do} first decreases with increasing T_1 for small values of K_{p1} (Figure 8(a)), reaches a minimum at around $T_1 = 1.1 \approx \pi/2\ \omega_{n1}$ and then increases again. The v_{do} curves for different K_{p1} values approximately intersect

each other at a value of T_1 around $(T_1)_{in} = 2.185 \approx \pi/\omega_{n1}$. These observations can be understood as follows. The stability boundary from the approximate results using the method of averaging (Equation (42a)) is given by

$$N_0 B_1 \omega_{n1} - \Psi_{11} K_{p1} \mu(v_d) \sin(\omega_{n1} T_1) = 0. \quad (49)$$

For the minima of the v_{do} vs. T_1 curve, we have $\partial v_d/\partial T_1 = 0$ which immediately implies from the above equation that $\cos(\omega_{n1} T_1) = 0$ or $T_1 = \pi/2\ \omega_{n1}$. Next, we note that the various stability boundaries of Figure 8 seem to intersect each other at $v_{do} = 0.2$ which is the critical velocity of the uncontrolled system ($(v_{do})_{un} = v_m = 0.2$). For this value, $B_1 = 0$ which requires $\sin(\omega_{n1} T_1) = 0$ or $T_1 = \pi/\omega_{n1}$ to satisfy Equation (49). For $0 < T_1 < (T_1)_{in}$, v_{do} decreases with increasing K_{p1}. Note that the critical disc velocity of the controlled system $v_{do} > (v_{do})_{un} = v_m$ for $T_1 > (T_1)_{in}$ making it an undesirable range for control applications. Owing to periodicity of the harmonic function, more regions of desirable T_1 values are obtained in the higher delay range. Another interesting phenomenon is observed when we use higher values of K_{p1} say 0.087. There is another disconnected branch of the v_{do} curve which appears in the low v_{do} range. Accordingly there is a range of T_1 values (0.8–1.3) for which the system is stable for very small v_d. It becomes unstable in the intermediate v_d range before stabilising further. This observation is in accordance with Figure 7(b) where two stability boundaries for two different v_d intersect at a particular point. With an increase in K_{p1} to 0.087506, these two branches meet approximately to form a cusp. A further increase in K_{p1} causes the branches to separate once again but the split this time involves higher and lower T_1 values. The minimum gap between the two branches signifying the 'completely stable region' where the system is stable for any disc velocity increases with increasing K_{p1}.

The above observations are further verified by plotting bifurcation diagrams with v_d as the bifurcation parameter as shown in Figure 9. The parameter values in Figure 9(a) are in accordance with Figure 8(a) (the dash-dotted line) while the parameter values in Figure 9(b) are in accordance with Figure 8(b) (the dotted line). We have used the software package DDE-biftool (Engelborghs et al. 2002) to plot these bifurcation diagrams with $\mathrm{sgn}(v_r)$ replaced by $\tanh(500\ v_r)$. It is observed from Figure 9(a) that only one bifurcation point v_{do} exists for $K_{p1} = 0.08$ and the amplitudes of the vibrations follow the same trend as v_{do}, i.e. initially decreasing with increasing T_1 until approximately 1.1 and increasing afterwards. However, we observe from Figure 9(a) that for $K_{p1} = 1.0$ an increase in T_1 induces two bifurcation points signified by two critical disc

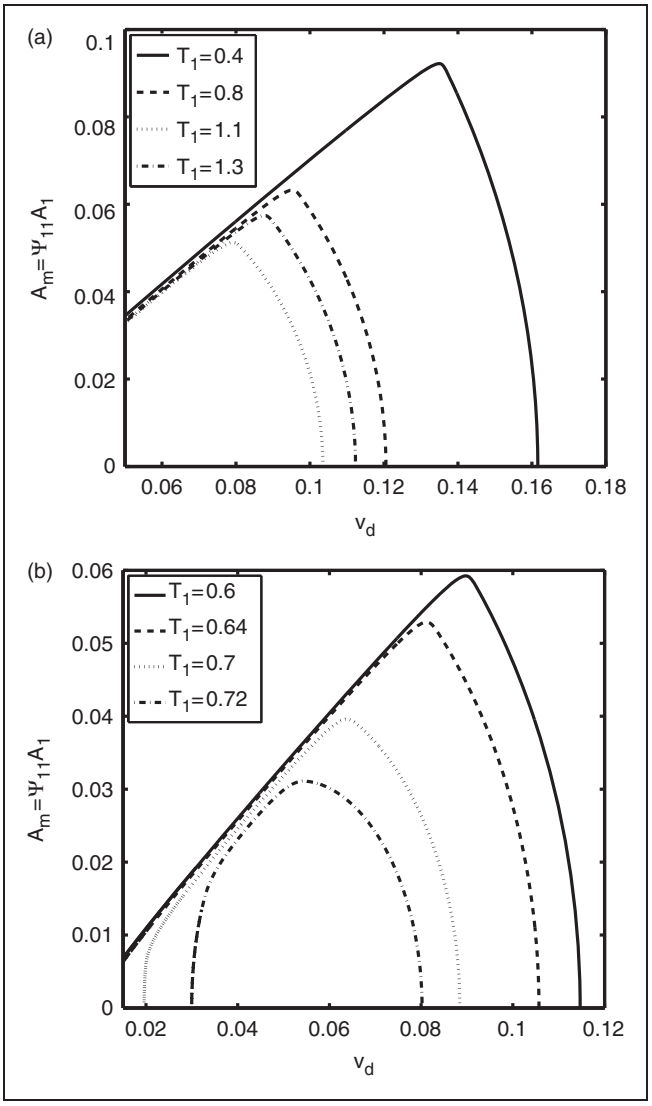

Figure 9. Bifurcation diagrams with v_d as the bifurcation parameter. Parameters: $\mu_s = 0.4$, $\mu_m = 0.25$, $v_m = 0.2$, $r_m = 0.8$, $N_0 = 0.02$ and $\kappa = 500$, with (a) $K_{p1} = 0.08$ and (b) $K_{p1} = 0.1$.

velocities v_{do1} and v_{do2} ($v_{do2} > v_{do1}$). Pure slipping limit cycles emerge from these points and are connected to each other by stick–slip limit cycles. The equilibrium is stable for $v_d < v_{do1}$ and $v_d > v_{do2}$.

We next consider the T_1 value of 1.1 corresponding to the 'completely stable region' and obtain some estimates of the maximum control forces that are required to achieve stability. To this end, we analyse some time-displacement relationships before and after the application of the control force as shown in Figure 10 for different K_{p1} values. The control force is applied at $\tau = 200$ for which the motion has settled to a stable stick–slip limit cycle of amplitude approximately 0.074. The variation of the corresponding control forces F_{c1} with time is plotted in Figure 11. It is observed from Figure 10

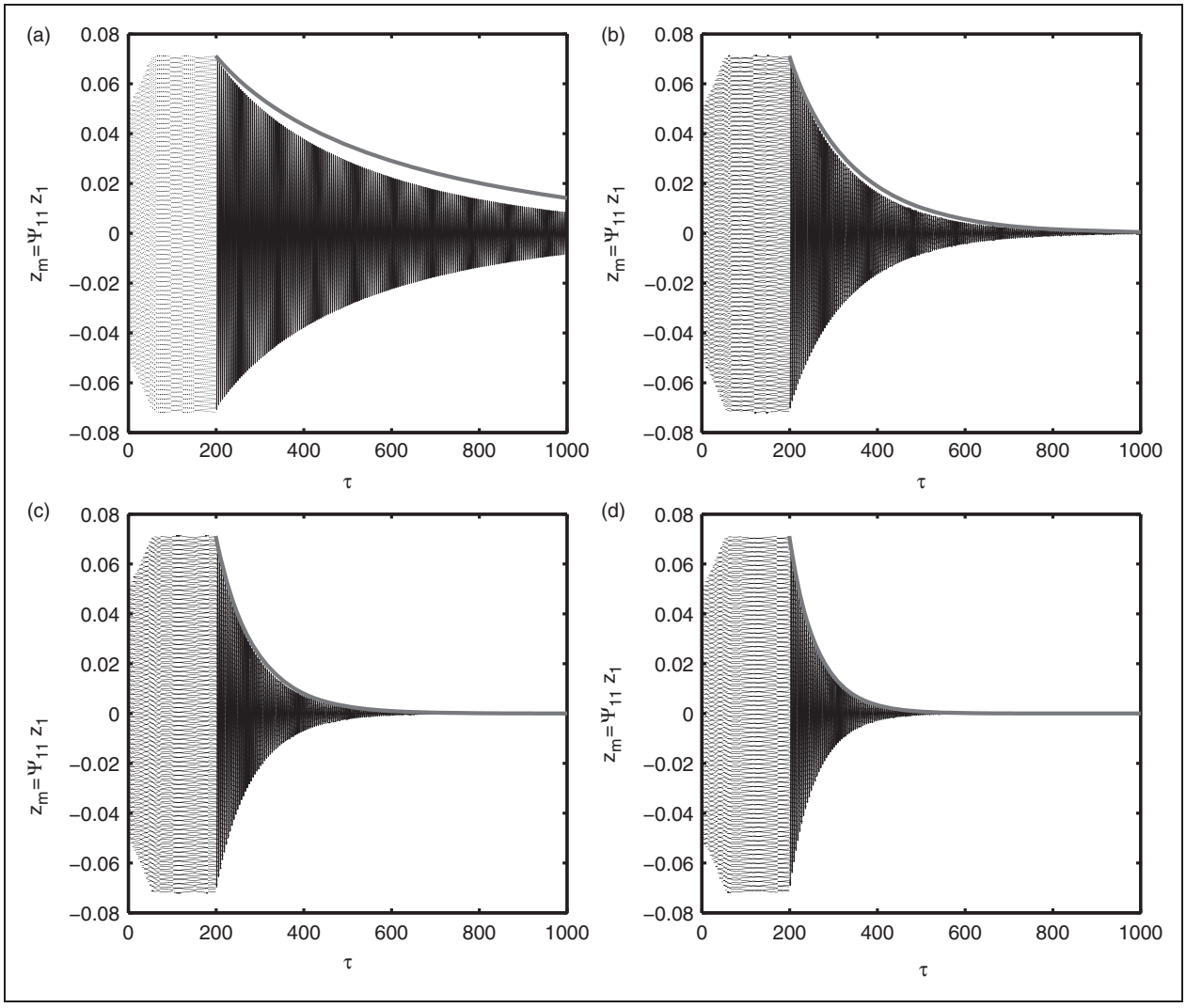

Figure 10. Evolution of the oscillations of the end mass (z_m) with time (τ) before and after the application of the control force. Parameters: $v_d = 0.1$, $\mu_s = 0.4$, $\mu_m = 0.25$, $v_m = 0.2$, $r_m = 0.8$, $N_0 = 0.02$, $\kappa = 500$ and $T_1 = 1.1$, with (a) $K_{p1} = 0.1$, (b) $K_{p1} = 0.15$, (c) $K_{p1} = 0.2$ and (d) $K_{p1} = 0.25$. The red thick lines denote the evolution of the amplitudes obtained using the method of averaging.

that the system stabilises quickly for higher K_{p1} values. However, this requires a higher initial control force as observed from Figure 11. For some cases (e.g. $K_{p1} = 0.25$) the extremal values of the control force $(F_{c1})_{\max}$ exceeds the pre-normal load N_0 in magnitude resulting in a momentary loss of contact between the end mass and the disc. This induces vibrations normal to the disc which might cause additional instabilities. Hence, very large values of K_{p1} are also not desirable. We have also plotted the evolution of the amplitudes obtained from the method of averaging in Figure 10 to check the validity of the averaging results. Note that the match is good for $K_{p1} = 0.15$, 0.2 and 0.25 while it does not match very well for $K_{p1} = 0.1$. This is possibly due to the fact that the value of 0.1 is very close to the exact stability boundary (see Figure 7) and the results from the averaging method are not very good in this regime due to the approximations involved (Saha et al., 2010).

6. Conclusions

We have analysed the dynamics and control of friction-induced oscillations due to the drooping characteristic of the friction force in a continuous system. We have considered a model consisting of a mass connected at the end of a cantilever beam which is in frictional contact with a rigid rotating disc. The mathematical model has been developed using the Euler–Bernoulli beam theory. The orthonormal mode shapes of a cantilever

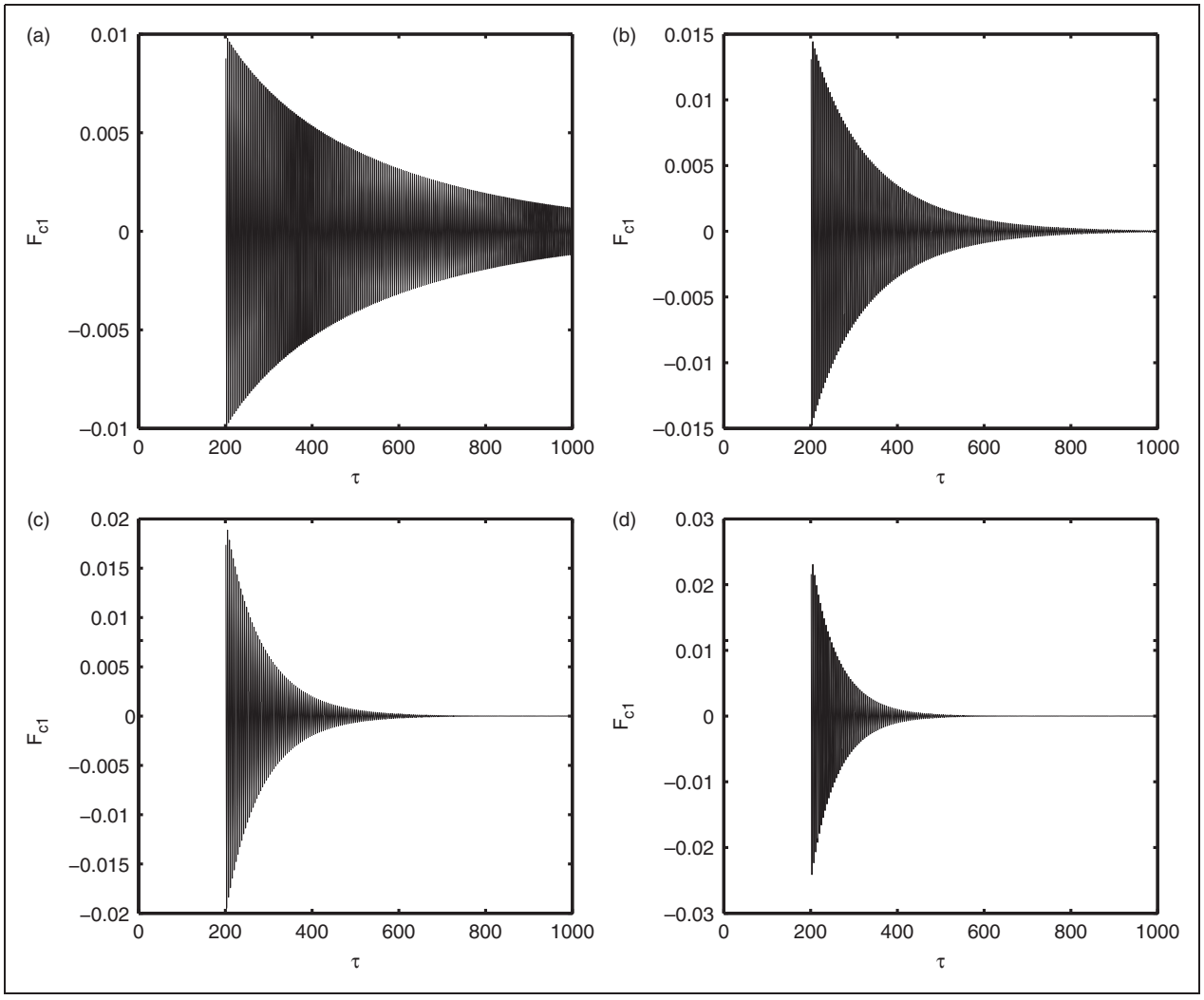

Figure 11. Variation of the control force with time (τ). Parameters: $v_d = 0.1$, $\mu_s = 0.4$, $\mu_m = 0.25$, $v_m = 0.2$, $r_m = 0.8$, $N_0 = 0.02$, $\kappa = 500$ and $T_1 = 1.1$, with (a) $K_{p1} = 0.1$, (b) $K_{p1} = 0.15$, (c) $K_{p1} = 0.2$ and (d) $K_{p1} = 0.25$.

beam with an end mass are utilised to reduce the partial differential equation governing the system to a set of ordinary differential equations. The dynamics of the uncontrolled system has been studied to obtain the parameter values satisfying the small deflection criteria for the validity of the beam equation. For these parameter values, the feasibility of controlling the vibrations using a time-delayed control force applied normal to the disc has been established. The stability boundaries corresponding to the Hopf bifurcation obtained using a linear analysis reveals the possibility of completely quenching the vibrations by an appropriate choice of control parameters. Desirable ranges of the control parameters for an effective control of vibrations have also been obtained. For certain choices of control parameters the controlled system has been found to be stable for low and high disc velocities but unstable for intermediate ones.

Funding

This work is supported by the Department of Science and Technology (DST), India (project number DST-ME-20090007).

References

Chatterjee S (2007) Time-delayed feedback control of friction-induced instability. *International Journal of Non-Linear Mechanics* 42: 1127–1143.

Das J and Mallik AK (2006) Control of friction driven oscillation by time-delayed state feedback. *Journal of Sound and Vibration* 297: 578–594.

Dunlap KB, Riehle MA and Longhouse RE (1999) *An Investigative Overview of Automobile Disc Brake Noise*. SAE Technical Paper, No 1999-01-0142.

Engelborghs K, Luzyanina T and Roose D (2002) Numerical bifurcation analysis of delay differential equations using

DDE-BIFTOOL. *ACM Transactions on Mathematical Software* 28: 1–21.

Felske A, Hoppe G and Matthäi H (1978) *Oscillations in Squealing Disc Brake Analysis of Vibration Modes by Hholographic Interferometry*. SAE Technical Paper, No. 780333.

Flint J and Hulten J (2002) Lining-deformation-induced modal coupling as squeal generator in a distributed parameter disc brake model. *Journal of Sound and Vibration* 254: 1–21.

Giannini O, Akay A and Massi F (2006) Experimental analysis of brake squeal noise on a laboratory brake set-up. *Journal of Sound and Vibration* 292: 1–20.

Giannini O and Massi F (2008) Characterization of the high-frequency squeal on a laboratory brake setup. *Journal of Sound and Vibration* 310: 394–408.

Hetzler H, Schwarzer D and Seemann W (2007) Analytical investigation of steady-state stability and Hopf-bifurcations occurring in sliding friction oscillators with application to low-frequency disc brake noise. *Communications in Nonlinear Science and Numerical Simulation* 12: 83–99.

Hinrichs N, Oestreich M and Popp K (1998) On the modeling of friction oscillators. *Journal of Sound and Vibration* 216: 435–459.

Hoffmann N, Fischer M, Allgaier R and Gaul L (2002) A minimal model for studying properties of the mode-coupling type instability in friction induced oscillations. *Mechanics Research Communicaitions* 29: 197–205.

Hoffmann N and Gaul L (2003) Effects of damping on mode coupling instability in friction induced oscillations. *ZAMM Zeitschrift fur Angewante Mathematik und Mechanik* 83: 524–534.

Hoffmann N and Gaul L (2010) The onset of friction-induced vibration and spragging. *Journal of Sound and Vibration* 329: 3537–3549.

Ibrahim RA (1994) Friction-induced vibration, chatter, squeal, and chaos: PartII: dynamics and modeling. *American Society of Mechanical Engineers* 47: 227–253.

Kelly SG (2000) *Fundamentals of Mechanical Vibrations*, 2nd edn. New York: McGraw-Hill Higher Education.

Kinkaid NM, O'Reilly OM and Papadopoulos P (2003) Review, Automotive disc brake squeal. *Journal of Sound and Vibration* 267: 105–166.

Matsuzaki M and Izumihara T (1993) *Brake Noise Caused by Longitudinal Vibration of the Disc Rotor*. SAE Technical Paper, No. 930804.

Murakami H, Tsunada N and Kitamura T (1984) *A Study Concerned with a Mechanism of Disc-Brake Squeal*. SAE Technical Paper, No. 841233.

Nakae T, Ryu T, Sueoka A, Nakano Y and Inoue T (2010) Squeal and chatter phenomena generated in a mounted bike disc brake. *Journal of Sound and Vibration* doi: 10.1016/j.jsv.2010.08.027.

Neubauer M, Neuber C and Popp K (2005) Control of stick–slip vibrations. In: *Proceedings of the IUTAM Symposium*. 18–22, July, Munich, Germany.

Neubauer M and Oleskiewicz R (2008) Brake squeal control with shunted piezoceramics—efficient modelling and experiments. *Proceedings of the Institution of Mechanical Engineers, Part D: Journal of Automobile Engineering* 222: 1141–1151.

Nishiwaki M, Harada H, Okamura H and Ikeuchi T (1989) *Study on Disc Brake Squeal*. SAE Technical Paper, No. 890864.

Ouyang H, Mottershead JE, Cartmell MP and Frishwell MI (1998) Friction-induced parametric resonances in discs: effect of a negative friction–velocity relationship. *Journal of Sound and Vibration* 209: 251–264.

Pandey SS (2010) Analysis and control of friction induced oscillations in an idealized brake model. MTech Thesis. Kanpur: Indian Institute of Technology.

Popp K and Rudolph M (2004) Vibration control to avoid stick–slip motion. *Journal of Vibration and Control* 10: 1585–1600.

Popp K and Stelter P (1990) Stick–slip vibrations and chaos. *Philosophical Transactions: Physical Sciences and Engineering* 332: 89–105.

Saha A, Bhattacharya B and Wahi P (2010) A comparitive study on the control of friction-driven oscillations by time-delayed feedback. *Nonlinear Dynamics* 60: 15–37.

Saha A and Wahi P (2010) Controlling the bifurcation in friction induced vibrations using delayed feedback. In: *Proceedings of the 9th IFAC Workshop on Time Delay Systems*. 7–9, June 2010, Prague.

Sanders JA, Verhulst F and Murdock J (2007) Averaging methods in nonlinear dynamical systems. *Applied Mathematical Sciences*. 59, Springer: Berlin.

Sheng G (2008) *Friction-Induced Vibrations and Sound: Principles and Applications*. Boca Raton, FL: CRC Press.

Shin K, Brennan MJ, Oh JE and Harris CJ (2002) Analysis of disc brake noise using a two-degree-of-freedom model. *Journal of Sound and Vibration* 254: 837–848.

Stelter P (1992) Nonlinear vibrations of structures induced by dry friction. *Nonlinear Dynamics* 3: 329–345.

Thomsen JJ (1999) Using fast vibrations to quench friction induced oscillations. *Journal of Sound and Vibration* 218: 1079–1102.

von Wagner U, Hochlenert D, Jearsiripongkul T and Hagedorn P (2004) Active control of brake squeal via smart pads. In: *Proceedings of the 22nd Annual Brake Colloquium*. Anaheim, CA: SAE Paper, No. 2004-01-2773.

Wahi P and Chatterjee A (2004) Averaging oscillations with small fractional damping and delayed terms. *Nonlinear Dynamics* 38: 3–22.

Wahi P and Chatterjee A (2008) Self-interrupted regenerative metal cutting in turning. *International Journal of Non-Linear Mechanics* 43: 111–123.